HHS Public Access

Author manuscript

Biomaterials. Author manuscript; available in PMC 2022 August 01.

Published in final edited form as:

Biomaterials. 2021 August ; 275: 120968. doi:10.1016/j.biomaterials.2021.120968.

An Adventitial Painting Modality of Local Drug Delivery to Abate Intimal Hyperplasia

Takuro Shirasu[#a], **Nisakorn Yodsanit**[#b], **Xiujie Xie**[#a], **Yi Zhao**[b], **Yuyuan Wang**[b], **Ruosen Xie**[b,c], **Yitao Huang**[a], **Bowen Wang**[a], **Go Urabe**[a], **Shaoqin Gong**[b,c,d,*], **Lian-Wang Guo**[a,e,**], **K. Craig Kent**[a,***]

[a]Department of Surgery, School of Medicine, University of Virginia, Charlottesville, VA, 22903, USA

[b]Department of Biomedical Engineering, and Wisconsin Institute for Discovery, University of Wisconsin-Madison, Madison, WI, 53715, USA

[c]Department of Material Science and Engineering, University of Wisconsin-Madison, Madison, WI, 53715, USA

[d]Department of Chemistry, University of Wisconsin-Madison, Madison, WI, 53715, USA

[e]Robert M. Berne Cardiovascular Research Center, University of Virginia, Charlottesville, VA, USA.

[#] These authors contributed equally to this work.

Abstract

A major medical problem is the persistent lack of approved therapeutic methods to prevent postoperative intimal hyperplasia (IH) which leads to high-rate failure of open vascular reconstructions such as bypass grafting. Hydrogel has been widely used in preclinical trials for perivascular drug administration to mitigate postoperative IH. However, bulky hydrogel is potentially pro-inflammatory, posing a significant hurdle to clinical translation. Here we developed a new modality of directly “painting” drug-loaded unimolecular micelles (UM) to the adventitia thus obviating the need for a hydrogel.

To render tissue adhesion, we generated amine-reactive unimolecular micelles with *N*-hydroxysuccinimide ester (UM-NHS) terminal groups to form stable amide bonds with the adventitia. To test periadventitial application, we either soaked balloon-injured rat carotid arteries in crosslinked UM-NHS (Mode-1) or non-crosslinked UM-NHS (Mode-2), or painted the vessel

[*] Corresponding author. Department of Biomedical Engineering, University of Wisconsin, Madison, WI, 53715, USA. shaoqingong@wisc.edu. [**] Corresponding author. Department of Surgery, School of Medicine, University of Virginia, Charlottesville, VA, 22903, USA. lg8zr@hscmail.mcc.virginia.edu. [***] Corresponding author. Department of Surgery, School of Medicine, University of Virginia, Charlottesville, VA, 22903, USA. ck8aq@hscmail.mcc.virginia.edu.

Declaration of interests

The authors declare that they have no known competing financial interests or personal relationships that could have appeared to influence the work reported in this paper.

surface with non-crosslinked UM-NHS (Mode-3). The UM-NHS were loaded with or without a model drug (rapamycin) known to be IH inhibitory. We found that Mode-1 produced a marked IH-mitigating drug effect but also caused severe tissue damage. Mode-2 resulted in lower tissue toxicity yet less drug effect on IH. However, the painting method, Mode-3, demonstrated a pronounced therapeutic effect (75% inhibition of IH) without obvious toxicity.

In summary, we present a simple painting modality of periadventitial local drug delivery using tissue-adhesive UM. Given the robust IH-abating efficacy and low tissue toxicity, this prototype merits further development towards an effective anti-stenosis therapy suitable for open vascular reconstructions.

Keywords

Intima hyperplasia; Perivascular application; Painting; Tissue adhesive unimolecular micelle

Introduction

Coronary artery disease, carotid artery disease, and peripheral artery disease share a common pathology of atherosclerosis, which affects around one third of adults and is a leading cause of death [1, 2]. The prevalence of atherosclerosis increases with age and is predicted to grow globally [1–3]. While endovascular approaches (e.g., stenting) are gaining momentum in current clinical managements of atherosclerosis, open surgical reconstructions such as bypass are often indispensable, especially in advanced stages of coronary and peripheral artery diseases [4]. However, lumen-narrowing intimal hyperplasia (IH) occurs, leading to recurrence of stenotic disease. To date, there is no IH-mitigating therapy clinically available to prevent postoperative failure of open surgical reconstructions [5–7].

With a long-term goal to meet this medical need, we previously developed a perivascular drug administration system using unimolecular micelles (UM) [8]. These nanoparticles consist of a hydrophobic “core” to provide high drug-loading capacity and sustained drug release, and a hydrophilic “shell” that enables solubility [8, 9]. To retain the soluble UM from flowing away from the desired area, we synthesized a thermosensitive phase-transition hydrogel to hold UM in the perivascular space. This UM/hydrogel hybrid system proved to be effective in hampering IH when applied periadventitially in a rat model [8–10]. However, potential issues remain, especially in the perspective of translation toward a clinical utility, such as the following: 1) The semi-solid hydrogel can be momentarily dislocated from the treatment site. 2) Once the UM-containing hydrogel decomposes, the UM will diffuse away. 3) Due to gel bulkiness, this UM/hydrogel system may not be applicable at some locations with limited perivascular space. 4) During the decomposition process of bulk hydrogel, local pH will decrease due to large amounts of acidic by-products, which would accelerate gel degradation while inciting inflammation [11, 12]. Thus, a new nanoplatform periadventitially applicable yet without needing the bulky hydrogel is highly desirable. Even more importantly, an easy and quick application mode is key to its translation to clinical use.

In this study, we innovated tissue-adhesive UM that can covalently link to the adventitia. We first tested periadventitial applications by soaking the vessel in a UM solution. To retain

drug loading capacity while omitting a bulky hydrogel, we crosslinked UM into a network (Mode-1) or applied non-crosslinked UM (Mode-2) for comparison. However, severe tissue fibrosis, inflammation, and cell death occurred in Mode-1, but not in Mode-2. Based on this finding, we conceived a simpler approach, to directly paint (pen brush) the vessel surface with non-crosslinked UM (Mode-3). To our surprise, while consuming only $^{1}/_{10}$ of drug-loaded UM, Mode-3 produced a pronounced IH-abrogating effect yet with minimized tissue toxicity. To the best of our knowledge, this is the first report of directly and covalently painting nanoparticles onto the adventitia to efficaciously and safely mitigate IH.

Materials and Methods

Materials

Rapamycin was purchased from LC Laboratories (Woburn, MA). Methoxy-PEG-NH_2 (mPEG-NH_2, M_n = 5 kDa), NH_2-PEG-OH (M_n = 5 kDa), maleimide-PEG-NH_2 (Mal-PEG-NH_2, Mn = 5 kDa), 4-arm PEG-NH_2 (M_n = 10 kDa), and 4-arm PEG-NHS (M_n = 10 kDa) were acquired from Biochempeg Scientific Inc. (Watertown, MA, USA). Cy5 dye was obtained from Lumiprobe Corporation (Hallandale Beach, FL, USA). Succinic anhydride, tin(II) 2-ethylhexanoate ($Sn(Oct)_2$), and 4-dimethylamino pyridine (DMAP) were purchased from Thermo Fisher scientific (Waltham, MA, USA). DSC was obtained from Oakwood Chemical (Estill, SC, USA). Anhydrous pyridine was acquired from EMD Millipore Corporation (Billerica, MA, USA). Other chemicals were obtained from Sigma-Aldrich (St. Louis, MO).

Preparation of tissue-adhesive UM-NHS

Synthesis of PAMAM-PVL-COOH—PAMAM-PVL-OH was first synthesized using PAMAM-OH (4^{th} generation, 31.50 mg, 6.33 μmol) and δ-valerolactone (411.19 μl, 4.43 mmol) through ring-opening polymerization with a catalyst, $Sn(Oct)_2$ (0.48 μL, 1.48 μmol) at 120°C for 24 hr as previously reported [8]. Then, PAMAM-PVL-OH (350 mg, 4.47 μmol, Mw 87.88 kDa) and succinic anhydride (279.88 mg, 2.80 mmol) were dissolved in anhydrous dichloromethane (DCM) (20 ml) before adding DMAP (427.10 mg, 3.50 mmol) [13]. The reaction was stirred at room temperature for 48 hr under N_2 atmosphere. To collect the product, the mixture was slowly precipitated in cold diethyl ether and centrifuged at 10,000 g for 10 min. The precipitate was purified by dialysis against DI water using a regenerated cellulose (RC) dialysis bag (molecular weight cut-off (MWCO) 15 kDa) for 48 hr, and lyophilized under vacuum.

Synthesis of Cy5-PEG-NH_2—Cy5-SH (5 mg, 7 μmol) was conjugated with Mal-PEG-NH_2 (29 mg, 5.8 μmol) in dimethyl sulfoxide (DMSO) (5 ml) through Michael addition [14]. The reaction was stirred at room temperature for 24 hr in the dark. Thereafter, it was purified by dialysis against DI water for 24 h using a RC dialysis bag (MWCO 2 kDa). The product was obtained after lyophilization under vacuum.

Synthesis of PAMAM-PVL-PEG-OCH_3/Cy5/OH (UM-OH)—PAMAM-PVL-COOH (100 mg, 1.28 μmol, Mw 87.88 kDa), NHS (33.90 mg, 294.58 μmol), and 1-ethyl-3-(3-dimethylaminopropyl) carbodiimide (EDC) (47.06 mg, 245.48 μmol) were first dissolved in

DCM (30 ml) to activate the carboxylic terminal, as reported [15]. mPEG-NH_2 (306.85 mg, 61.37 μmol, 5 kDa), HO-PEG-NH_2 (306.85 mg, 61.37 μmol, 5 kDa), and NH_2-PEG-Cy5 (25.57 mg, 5.11 μmol, 5 kDa) were then added into the reaction. The reaction was stirred at 4°C to RT for 48 hr under N_2 atmosphere in the dark. The crude product was collected by precipitation in cold diethyl ether and dialyzed against DI water using a RC dialysis bag (MWCO 15 kDa) for 48 hr in the dark before lyophilization to obtain UM-OH.

Synthesis of PAMAM-PVL-PEG-OCH $_3$/Cy5/NHS ester (UM-NHS)—PAMAM-PVL-PEG-OCH_3/OH/Cy5 (120 mg, 0.50 μmol, Mw 247.88 kDa) was dissolved in DCM. Then, DSC (10.32 mg, 20.15 μmol) and anhydrous pyridine (5.0 μl, 30.22 μmol) were added into the mixture in order to generate NHS terminal [16]. The reaction mixture was stirred at room temperature for 24 hr in the dark. To remove unreacted PEG and DSC, the solution was dialyzed against DCM using a RC dialysis bag (MWCO 15 kDa) for 24 hr and precipitated in diethyl ether. The precipitate was then lyophilized to yield UM-NHS, which was then stored in the dark.

Preparation of rapamycin-loaded UM-NHS—UM-NHS (60 mg) and rapamycin (20 mg) were dissolved in DMSO (5 ml). DI water (15 ml) was added dropwise into the mixture to provide rapamycin-loaded UM-NHS, as previous reported [8]. The unloaded rapamycin was removed by dialysis against DI water using a RC dialysis bag (MWCO 15 kDa) for 24 hr before lyophilization.

Characterization of UM-NHS

The chemical structures and molecular weights were determined by the ^{1}H NMR spectroscopy (Bruker Avance-400 MHz) (Figure S1), and gel permeation chromatography equipped with triple detectors (GPC, Viscotek, Malvern), respectively [17]. The NMR samples were prepared in deuterated chloroform ($CDCl_3$) (~5 mg/ml) while the samples for GPC analysis were dissolved in dimethylformamide (DMF) (~0.5 to 1.0 mg/ml). Fourier-transform infrared (FTIR) spectroscopy (Tensor 27, Bruker) was used to confirm the carboxylic acid at the terminal in PAMAM-PVL-COOH, and NHS functional groups in UM-NHS. The hydrodynamic diameter and zeta-potential of UM-NHS were measured using a dynamic light scattering (DLS) machine (Zetasizer NanoZS90, Malvern). For diameter measurement, PAMAM-PVL-OH and PAMAM-PVL-COOH were dispersed in chloroform (0.02 mg/ml), while UM-NHS was suspended in DI water (0.02 mg/ml). For zeta potential measurement, all samples were dispersed in DI water (0.02 mg/ml) (Figure S2). Additionally, morphology of UM-NHS was observed under transmission electron microscope (TEM, FEI Tecnai TF-30) using phosphotungstic acid (PTA) as a negative stain. To prepare the TEM sample, the UM-NHS solution (0.05 mg/ml in DI water) was dropped onto a TEM grid (Formvar/Carbon coated copper grids, 200 mesh). The grid is air dried and a drop of PTA solution (1%, pH 7) was added onto the grid. After 30 seconds, excessive PTA solution was removed by a filter paper, and the grid was air dried. The rapamycin loading content was quantified by HPLC (Elite LaChrom, Hitachi) at 278 nm using 0.5 mg/ml of drug-loaded UM-NHS in DMSO [8].

Quantification of rapamycin release from UM-NHS in vitro

The rapamycin release profiles from Mode-1 (UM-NHS with gel), Mode-2 (UM-NHS), and Mode-3 (UM-NHS) were measured following the reported protocol [8] with some modifications. In Mode-1, UM-NHS (1 ml, 250 mg/ml in $NaHCO_3$ buffer, pH 8), 4-arm For Mode-1, PEG-NHS (0.75 ml, 320 mg/ml in $NaHCO_3$ buffer, pH 8) and 4-arm PEG-NH_2 (0.75 ml, 320 mg/ml in $NaHCO_3$ buffer, pH 8) were mixed and enclosed in a RC dialysis bag (MWCO 8 kDa). For Mode-2 and Mode-3, UM-NHS (1 ml, 250 mg/ml in $NHCO_3$, pH 8) was stored in the same type of dialysis bag (MWCO 8 kDa). The dialysis bags were then immersed in PBS (25 ml, pH 7.4) with 0.2% tween80 and kept in a horizontal shaker (140 rpm) at 37°C. At the time points indicated in the figure legend, supernatants (1 ml) were collected and replaced with fresh media (1 ml). The amounts of rapamycin in the supernatants were quantified by HPLC at 278 nm.

Animals

All animal experiments were carried out in accordance with the *Guide for the Care and Use of Laboratory Animals* (National Institutes of Health), and the protocols are approved by the Institutional Animal Care and Use Committee of University of Virginia. Sprague-Dawley rats were purchased from Charles River Laboratories (Wilmington, MA). Females differ from males in body structure and artery size which affect the IH-inducing open surgery. To omit this confounding variable, we used only male rats for experiments (300 – 330 g body weight). They were kept in isolation racks in an air-conditioned room with 12 hr - 12 hr light-dark cycle, fed with a normal diet, and free to access food and water.

Model of open surgery of rat carotid artery balloon injury to induce IH

Balloon injury was performed as previously described [18, 19]. In brief, rats were anesthetized with inhalation of isoflurane (5% for induction and 2% for maintenance), a midline incision was made in the neck, and carotid arteries were dissected. A 2-Fr. balloon catheter was inserted via an arteriotomy on the external carotid artery, and the entire length of common carotid artery (CCA) was injured by withdrawing the balloon catheter inflated at 1.5 atm. The balloon was withdrawn straight 3 times, while at the 4^{th} time retracted with rotation. In all surgeries, the omohyoid muscle was resected when dissecting carotid arteries, and sternocleidomastoid muscle was also resected at the time of periadventitial crosslinked-UM application. Bupivacaine (up to 8 mg/kg) was locally injected at the incision site, and carprofen (5mg/kg) and buprenorphine (0.05 mg/kg) were subcutaneously injected after the surgery. The rats were euthanized 14 days after surgery and CCAs were collected after perfusion fixation with 4% paraformaldehyde (PFA). The collected arteries were fixed in 4% PFA for 12–24 hr, paraffin-embedded, and then processed for morphometric analysis.

Periadventitial application of rapamycin-encapsulated UM-NHS

The UM-NHS nanoparticle as a drug carrier was applied in 3 different modes. In Mode-1, UM-NHS were crosslinked into a network. PEG-based gels with NHS and amine (-NH_2) terminal groups, that are commonly used for sealant [20], are utilized to form the crosslinked system. As illustrated in Figure 1A, the 4-arm PEG-NH_2 (10 kDa) can react with both UM-NHS and 4-arm PEG-NHS (10 kDa) to form a network. For each rat, 250 mg/ml

UM-NHS (120 μl), 320 mg/ml of 4-arm PEG-NH_2 (90 μl), and 320 mg/ml of 4-arm PEG-NHS (90 μl) were first prepared in $NaHCO_3$ buffer with a pH value of 8. These components were mixed right before perivascular application. In Mode-2, UM-NHS were not crosslinked and remained in solution (250 mg/ml in $NaHCO_3$ buffer, pH 8) until periadventitial application (Figure 1B). In these two modes, immediately after balloon injury of the CCA, UM-NHS (crosslinked or non-crosslinked) were contained in a cup formed with a Parafilm membrane (Bemis Company, Inc, Neenah, WI) around the injured artery. In Mode-1, we observed solidification of the components (~1 min), while in Mode-2, we incubated the arteries for 15 min and gently rinsed the outer surface of the arteries with PBS. Cy5 Fluorescence imaging confirmed the presence of UM-NHS even 14 days after the periadventitial application (Figure S3). In Mode-3, the CCA was quickly rinsed with PBS drops, and cleaned with gauze. A pen brush (Sable Brushes, size 4, Solo Horton Brushes, Inc., Winsted, CT) was then used to dip into the non-crosslinked UM-NHS solution (250 mg/ml in $NaHCO_3$ buffer, pH 8) and to paint the solution throughout the surface of the injured artery (Figure 1B). The painting process was completed in 30 seconds. The excess solution on the artery was immediately removed with gauze. For each periadventitial application mode, empty UM-NHS (no rapamycin loaded) was used as no-drug control for rapamycin-loaded UM formulations. Weights of the painted UM-NHS solution were measured every time.

Morphometric analysis of IH

One rat in treated group with empty UM-NHS group was excluded due to thrombotic occlusion. At 14 days after balloon injury, CCAs were collected. Each CCA embedded in paraffin was cut into 3 segments: proximal, middle, and distal. At least 4 sections (each 5 μm thick) representing different locations were cut from these segments for morphometric analysis. The sections included two from the proximal and distal ends of CCA and the other two from the ends of the middle segment. These specimens were processed for hematoxylin-eosin and Masson's trichrome staining. Morphometric analysis was conducted using Image J software (NIH, Bethesda, MD, USA). Lumen area, area inside internal elastic lamina (IEL), area inside the outer boundary of adventitia together with lumen and IEL perimeters were determined. Calculations were conducted as follows; intimal area = IEL area - lumen area; standardized intimal thickness, intima area/IEL perimeter; stenosis rate, (intima area/IEL area)*100; intima/media ratio (I/M ratio), intima area/(area inside adventitia - IEL area). The values from 4–6 CCA sections were averaged to produce a mean for each animal, and the means from all animals in each group were averaged again to calculate mean ± SEM (standard error of mean). To observe the localization of Cy5-labelled UM, snap frozen samples were used, and examined under fluorescent microscope.

Quantification of collagen density in the artery

Four to six cross-sections cut from different locations (see detailed description above) from the balloon-injured CCA per each animal were used for Masson's trichrome staining. The color images were transformed into monochrome images at an 8-bit scale using Image J. After adjusting the threshold consistent through the analysis, integrated density of interest was measured. Data values from 6 sections were averaged for each animal, and averages from total animals in a group were used to calculate mean + SEM and statistical analysis.

Immunohistochemistry analysis of tissue toxicity

Paraffin-embedded specimens were processed into 5-μm thick sections for immunostaining. The slides were deparaffinized and hydrated through series of xylenes and graded alcohol. Antigens were retrieved using citrate buffer for 2 hours at 80°C in a high-pressure cooker. Endogenous peroxidase was blocked by incubation with 3% H2O2 for 10 min. Following the application of a monoclonal antibody against either cleaved Caspase 3 (1:400 dilution) (9661, Cell Signaling Technology, Inc., Danvers, MA) or CD68 (1:100 dilution) (T-3003, BMA Biomedicls, Augst, Switzerland), an anti-rabbit secondary antibody was used, which was included in the ImmPRESS Polymer HRP (peroxidase) detection kit (MP-7451, Vector Laboratories Inc., Burlingame, CA). The staining intensity was visualized using ImmPACT DAB Peroxidase (HRP) Substrate (SK-4105, Vector Laboratories). Data values from 6 different portions were averaged for each animal, and averages from total animals in a group were used to calculate mean + SEM and statistical analysis.

Statistical analysis

Data sets were subjected to normality check using Shapiro–Wilk test. Student's t-test was used for two group comparison; one-way analysis of variance (ANOVA) was performed for multiple group comparison followed by post hoc test (specified in figure legends). All data are presented as mean ± standard error of the mean (SEM). A difference is considered statistically significant when a p value is < 0.05.

Results

Preparation and characterization of UM-NHS

PAMAM-PVL-OH was prepared via ring-opening polymerization as described previously [8], and then reacted with succinic anhydride under basic pH to yield PAMAM-PVL-COOH. The ^{1}H NMR spectra of both products showed characteristic peaks at δ 4.08, 2.34, and 1.67 ppm, assigned to the methylene protons in PVL, and at 3.65 ppm as terminal methylene protons in PVL (Figure S1A, S1B) as previously reported [8, 13, 17]. Additionally, the average number of repeating units of the PVL was calculated to be 23, based on the area ratio of the peaks at (c) 4.08 ppm and (c') 3.65 ppm (Figure S1A). The hydrodynamic diameters of PAMAM-PVL-OH and PAMAM-PVL-COOH were 23.0 ± 2.4 and 24.6 ±3.4 nm, respectively. However, the zeta potential of PAMAM-PVL-OH was almost neutral (1.28 ± 1.01 mV) while that of PAMAM-PVL-COOH was negative (−22.97 ± 0.99 mV), which can be attributed to the carboxyl terminal groups (Table S1). Furthermore, FTIR spectra of PAMAM-PVL-OH and PAMAM-PVL-COOH were studied. C=O stretching of carbonyl (1726 cm^{-1}) was found in both compounds due to PVL segments while anti-symmetric C=O stretching of carboxyl (1552 cm^{-1}) was only observed in PAMAM-PVL-COOH (Figure S2C) [21, 22]. Next, PAMAM-PVL-COOH was activated by EDC-NHS, followed by PEGylation with amine-PEG-OCH_3/Cy5/OH to produce PAMAM-PVL-PEG-OCH_3/Cy5/OH (UM-OH) [16]. Then, hydroxy at the terminal of UM-OH was reacted with the carbonyl group in DSC to generate PAMAM-PVL-PEG-OCH3/Cy5/NHS (UM-NHS) under basic condition (Figure 2). We found that the hydrodynamic diameter of UM-NHS was about 65.66 ± 5.73 nm, and the zeta potential became neutral (~1.50±0.84 mV) (Table S1, Figure S2A). Additionally, the diameter of the spherical UM-NHS nanoparticle

measured by TEM was around 63 nm (Figure S2B). The chemical structures of UM-OH and UM-NHS were characterized by ^{1}H NMR. The peaks at δ ~6.5–7.0 and 3.64 ppm indicated the conjugation of Cy5 and PEG, respectively (Figure S1C, S1D) [17]. The NMR characteristic peak of NHS ester was shown at δ 2.84 ppm in UM-NHS [23]. Additionally, FTIR was used to confirm the presence of NHS, which was found at 1637 cm^{-1} (N-O stretching) and 1778 cm^{-1} (C=O stretching; anhydride) from UM-NHS, but not in the UM-OH (Figure S2D) [24].

Rapamycin release Profiles from UM-NHS in vitro

The rapamycin loading content in UM-NHS was 20.3 wt%, which was measured by HPLC following our previously reported method [8]. Figure S2E shows two release profiles, from crosslinked (corresponding to Mode-1) and non-crosslinked UM-NHS (Mode-2 and Mode-3), with 38.3% and 83.6% release at Day 60 from the crosslinked and non-crosslinked delivery system, respectively. The release from the crosslinked delivery system was retarded probably due to a drug-trapping effect of the crosslinked network, similar to the UM encapsulated in a hydrogel [25].

Periadventitial drug delivery using crosslinked and non-crosslinked UM-NHS for IH mitigation

To evaluate the utility of tissue-adhesive UM for periadventitial local drug delivery, we opted to use the well-established model of rat carotid artery balloon angioplasty that robustly induces IH. Upon surgery, the rat neck needs to be opened through an incision in order to dissect out the carotid arteries. As such, this model resembles open vascular surgery, and hence meets our purpose of testing perivascular application of the UM formulations for their IH-mitigating efficacy. We used rapamycin as an IH-inhibitory model drug, which is established in both pre-clinical and clinical settings.

To eliminate a hydrogel that was used in our previous studies to sequester nanoparticles in the periadventitial space, we first crosslinked UM-NHS into a network to retain a high drug-loading capacity (Mode-1). For comparison, an equal amount of UM-NHS (non-crosslinked) was used, which remained as a UM nanoparticle liquid solution during the periadventitial application (Mode-2). To ensure sufficient conjugation of UM-NHS with the NH_2 group on the adventitial matrix proteins, we soaked (incubated) the balloon-injured carotid artery in UM-NHS (crosslinked in Mode-1; non-crosslinked in Mode-2) for 15 min, in a reservoir formed around the artery with a Parafilm membrane. In each mode, the empty UM formulations (no drug) were used as a control against the rapamycin-loaded UM. At 14 days post-surgery, animals were euthanized for morphometric analysis of IH and tissue toxicity evaluations through immunohistochemistry.

To measure IH, we primarily used the intima versus media area ratio (I/M). We also normalized the intima area to IEL length, termed as normalized intima thickness (NIT), taking advantage of the fact that IEL length, unlike IEL area, is not subject to the variability caused by morphological deformation of the artery cross sections. Moreover, stenosis rate was also calculated (Figure 3). We used these three parameters to evaluate IH. In Mode-1, the I/M ratio, NIT, and stenosis rate were significantly reduced (with *vs* without rapamycin)

by 74.6% (from 0.90 ± 0.12 to 0.23 ± 0.03), 77.4% (from 68.3 ± 8.9 to 15.4 ± 3.3), and 67.9% (from 37.5 ± 5.2% to 12.0 ± 1.4%), respectively, yet the lumen area did not change. In Mode-2, IH was also inhibited by the rapamycin-loaded UM (*vs* no drug). The I/M ratio, NIT, and stenosis rate significantly decreased (with *vs* without drug) by 53.8% (from 0.94 ± 0.04 to 0.43 ± 0.05), 51.3% (from 67.9 ± 3.8 to 33.1 ± 4.5), and 53.1% (from 40.4 ± 2.7% to 18.9 ± 2.7%), respectively. The lumen area increased significantly by 42.9% (from 238465 ± 18301 to 340728 ± 18192). Since the stenosis rate is also subject to changes of overall vessel size, we assessed it by measuring the length of external elastic lamina (EEL). Indeed, the EEL length in Mode-1 decreased (no statistical significance), which could account for the lack of increased lumen area even though the neointima was markedly reduced. By contrast, the vessel size in Mode-2 increased albeit without reaching statistical significance. Thus, while IH was mitigated to a greater extent in Mode-1 than in Mode-2, a desired increase of lumen area occurred in Mode-2 but not in Mode-1.

Tissue toxicity of crosslinked UM-NHS after periadventitial application

During the experiment, we noticed a bulging of the animal neck in Mode-1 but not in Mode-2 (Figure 4). Upon tissue collection at the end of the Mode-1 experiment, we observed that the CCAs were buried in scar tissues and hardly dissectible, a problem that did not occur in Mode-2 (Table S2). Consistently, histology showed that the arteries from Mode-1 but not Mode-2 appeared to be tightly connected with surrounding tissues, suggestive of tissue fibrosis (Figure 4A). We thus performed Masson's trichrome staining to evaluate collagen accumulation in the vessel wall. Indeed, severe fibrosis occurred in Mode-1 in comparison to Mode-2 (the empty UM condition), as indicated by much intensified adventitial collagen accumulation (Figure 4B, 4C). Rapamycin alleviated this fibrotic severity in Mode-1, a finding consistent with the previously reported anti-fibrotic effect exhibited by rapamycin [26].

Considering that tissue fibrosis is often associated with inflammation, we next determined macrophage infiltration via immunostaining of the marker CD68. In agreement with the above observations, the number of CD68-positive cells of the Model-1 empty UM condition was the highest across all conditions in Mode-1 and Mode-2. While this number was significantly higher above the injury-only background control either in the adventitial or medial layer or when counted in all layers (Figure 5), the difference was abolished by rapamycin in Mode-1. Compared to the Mode-1 empty UM condition, CD68 staining in Mode-2 remained significantly lower. In the neointima layer, no significant difference in CD68 staining was seen across all conditions. The number of cells stained positive for activated (cleaved) caspase-3 was significantly higher in the neointima layer in Mode-1, either compared to no treatment control or Mode-2. In other layers, while there appeared to be more apoptotic cells in the Mode-1 empty UM condition than other conditions, the differences were not significant.

Taken together, the above results indicated that Mode-1 but not Mode-2 produced a significant IH-mitigating therapeutic effect. However, the severe tissue damage imposed by this crosslinked UM drug delivery platform is prohibiting for further translation.

Adventitial painting of non-crosslinked UM-NHS for effective non-toxic mitigation of IH

To create a simple, non-toxic modality for anti-IH periadventitial drug application, we sought for further improvement based on Mode-2, which proved to be less toxic than Mode-1. Since the soaking approach requires extra time and materials for preparation and a Parafilm reservoir which nonetheless is subject to spill of the UM-NHS solution, we replaced it with direct painting of non-crosslinked UM-NHS over the artery outer surface. In addition, as the NHS-ester/NH_2 reaction is known to occur rapidly and robustly under basic condition, we eliminated the 15-min incubation step used in the soaking approach.

Instead, we used a pen brush to dip into the non-crosslinked UM-NHS solution and painted it onto the outer surface of the injured carotid artery (Mode-3). The entire painting process took less 30 seconds. It was interesting to note that only $^1/_{10}$ of the UM-NHS solution was consumed as compared to the soaking approach (Mode-2). To minimize quenching of UM-NHS by NH_2-containing molecules (e.g., soluble proteins) in the body fluid, the artery was pre-cleaned prior to painting. To prevent unreacted free UM-NHS or the byproduct (NHS) from diffusing into the surrounding tissues, the artery surface was gently cleansed with gauze immediately after painting. As indicated by the Cy5 fluorescence, UM was effectively sequestered in the adventitial layer after cleaning with gauze (Figure 6A). Cy5 fluorescence remained visible in the adventitial layer 7 days after application. The fading of fluorescence could be due to quenching, or loss of the Cy5 group possibly due to the hydrolytic and enzymatic cleavage of the ester bond linking the PEG arms onto the UM.

Importantly, morphometric analysis showed that a remarkable IH-mitigating effect was achieved through this painting approach (Figure 6). The I/M ratio was decreased by 75.5% (from 1.50 ± 0.37 to 0.37 ± 0.04) in the animal group applied with rapamycin-loaded UM-NHS compared to the empty UM control. Similarly, the NIT and stenosis rate were reduced by 68.9% (from 86.5 ± 17.1 to 26.9 ± 3.7) and 66.6% (from 49.2 ± 11.2% to 16.4 ± 2.1%), respectively. In accordance, the lumen area increased by 37.7% (from 244743 to 336968) albeit without reaching statistical significance ($p = 0.12$). The EEL length also increased, though without reaching statistical significance.

The next important question concerned the potential toxicity of the adventitial modification by UM-NHS (regardless of drug loading). Compared to the un-treated group (no adventitial modification), painting with empty UM-NHS did not increase the inflammation and apoptosis markers in any of the artery tissue layers. Instead, UM-NHS reduced apoptosis in the adventitial layer (Figure 7).

Rapamycin reduced CD68 staining in the vessel wall, and also lowered the overall number of caspase-3 positive cells, as compared between the conditions with and without drug loaded. Thus, Mode-3 appeared to be a highly desirable approach for periadventitial drug delivery, although it is not directly comparable to Mode-2 considering that these two modes were performed at different times, multiple variables between these experiments, including incubation time (30 seconds versus 15 min) and application method (painting versus soaking). Moreover, since macrophage infiltration occurs early following arterial injury and the inflammation reaction may resolve later, the assays using specimens collected at Day14 may not capture such early-phase events. Nonetheless, we found that Mode-3 provides an

easy and quick application to efficaciously stymie IH progression. To further test the efficacy of Mode-3 for a longer term, we performed another set of experiments and collected arteries at 1 month after surgery (Figure S4). The I/M ratio, NIT, and stenosis rate decreased (with *vs* without drug) significantly by 40.4% (from 1.03 ± 0.07 to 0.61 ± 0.04), 35.8% (from 59.5 ± 5.7 to 38.2 ± 2.5), and 43.7% (from 36.3 ± 4.1% to 20.4 ± 1.3%), respectively. The lumen area significantly increased by 41.7% (from 257089 ± 30104 to 364264 ± 7553). The overall vessel size (EEL length) was slightly enlarged although the change was not statistically significant ($p = 0.14$).

Discussion

We report here a simple modality of drug delivery aimed at perivascular application to mitigate IH following surgical vascular reconstructions. The delivery platform is a unimolecular micelle (UM) with NHS ester terminal groups that enable tissue-adhesion. Its periadventitial application is simple, requiring only a pen brush, and quick, within 30 seconds. Yet, the therapeutic outcome is remarkable, with a 75% decrease of IH without obvious tissue damage. Thus, the most prominent feature of this prototype is its simplicity, efficacy, and safety. Given an estimated ~15 to 70% of 1-year failure rate of open vascular reconstructions [6, 7, 27–29] for which no preventive measures are clinically available, this prototype merits further development.

Open surgical procedures remain a major approach for vascular reconstruction. These mainly include coronary artery bypass graft surgery, vein grafting for peripheral arteries, and renal dialysis access, collectively accounting for over 1 million cases annually in the US alone [1, 30, 31]. Unfortunately, there remains a lack of effective methods to prevent these grafts from post-operation failure which primarily results from IH [5–7]. One potential option to prevent vein graft failure is external stents to mitigate IH by appropriating the turbulent flow [32]. However, this method is ineffective for the perianastomotic lesions at the two ends of the graft where IH is particularly severe, occurring in the crucial period of 1–24 months after grafting [6]. In fact, the first trial of external stent revealed worsened patency at anastomotic lesions compared to the non-stent group [32]. Clearly, there remains a critical medical need for a perivascular drug delivery method that is particularly suited for IH-mitigating therapy following open vascular surgery.

Our previous endeavors led to a UM/hydrogel delivery system for open surgery that proved effective in restricting IH in a rat model [8, 10]. Bulky hydrogel was required to keep UM in place after perivascular application. However, the gel is subject to dislocation and it also evokes inflammation upon decomposition. To resolve these major shortcomings, we conceived a gel-free painting paradigm to immobilize UM directly onto the adventitia through stable covalent bonds.

To our knowledge, a painting method has not been previously reported for periadventitial applications to treat IH. In other applications (e.g., skin wound healing), various tissue-adhesive molecules have been tried, including aldehydes, biotin/avidin, and a collagen-binding fibronectin domain [33–37]. However, limitations exist, particularly thinking of clinical applications that impinge on the tender vascular tissues proximal to vital organs such

as heart, where the toxicity of aldehydes is a grave concern [33]. While the biotin/avidin pair features high binding affinity and low toxicity, neither biotin nor avidin is tissue-adhesive[34]. Although fibronectin adheres to collagen-containing tissues, the binding is non-covalent and hence unstable; moreover, a fibronectin domain *per se* is a signaling molecule that possibly elicits pro-IH complications [35, 36]. Catechol-based adhesives represent another important bioinspired adhesive technology [37]. However, the underlying Dopa chemistry submits to influences of redox, pH, metal ion chelating, and surface drying condition etc., and to a propensity of crosslinking into polymers (herein unwanted, as demonstrated by Mode-1). As such, this technology demands stringent control of the microenvironment. We chose NHS ester for covalent UM-tissue bonding because of the following main advantages [38–40]:

1) NHS ester is highly desired in protein conjugation applications for its quick robust reaction with the NH_2 group; 2) the reaction generates an amide bond, which is relatively stable; 3) the by-product, NHS, is generally regarded as minimally toxic [38] and can be easily cleansed, as herein demonstrated using gauze. It is thus not a surprise that NHS esters have been widely used in protein industry and bioengineering applications.

When initially designing the Mode-1 periadventitial UM-NHS application, we prioritized drug-loading capacity. A crosslinked UM network enabled loading of 6 mg of rapamycin for each animal, a dosage expected to markedly reduce IH based on our previous report [8]. Unfortunately, we observed severe tissue-damaging side effects, as evident from the fibrotic, inflammatory, and apoptotic markers in the adventitial and periadventitial tissues. Since this occurred in both animal groups receiving crosslinked UM with or without rapamycin, we suspected that UM crosslinking *per se* might be a problem. Indeed, implanted synthetic polymers with a significant mass are often recognized as “alien” by the immune systems, and inflammatory/fibrogenic responses may hence set off [41]. Moreover, the rigidity of a crosslinked network may impose mechanic stress on the vessel promoting inflammation/fibrosis [41, 42]. By contrast, tissue damage was markedly ameliorated in Mode-2, where UM-NHS alone rather than a bulky crosslinked network was applied. We further noticed that by soaking the vessel for extended time in Mode-2, UM-NHS might over-react with the tissue potentially causing harm. We were therefore prompted to use a painting approach (Mode-3) for a faster and cleaner UM-NHS application.

The Mode-3 application is quick (completable in 30 seconds) and requires much less rapamycin-loaded UM-NHS (only ~ $^1/_{10}$ of that used in Mode-2). Yet, the outcome from Mode-3 was superior: a 75% reduction of IH and nearly undetectable tissue damage. There are several possible explanations for this. First, quick painting followed by immediate removal of excess UM-NHS solution could avoid damage of overreaction with tissues. Second, without forming a crosslinked network, the small sized (~50 nm in diameter) individual UM-NHS molecule/nanoparticle can readily infiltrate into the adventitia. In contrast, the crosslinked network (Mode-1) cannot infiltrate but rather acts as a rigid “cast” that impinges on the vessel thereby prompting damage. Third, the adventitia is essentially a “sponge” composed of various scaffolding extracellular matrix proteins such as collagen, elastin, and fibrillin fibers, which confer extended surface area for UM’s covalent attachment via the NHS ester/NH_2 reaction [43]. As such, the UM conjugated onto the

adventitia constitute a drug reservoir, with a much larger volume than it would appear to be if calculated based on the outer surface of the vessel. Last yet importantly, with the durable UM slowly and locally releasing rapamycin into the adjacent media/intima layer, the minimal effective drug dosage can be substantially reduced [8].

Therefore, this Mode-3 direct painting modality of local drug delivery appears to meet the basic criteria for translatability to the clinical setting. 1) Mode-3 is highly effective in hampering IH with low rapamycin dosage. 2) This method appears to be tissue-friendly without causing obvious damage. 3) It provides local delivery to minimize systemic complications. 4) The UM nanoparticle has excellent stability in comparison with self-assembled multimolecular nanoparticles since the UM nanoparticle is formed by a single molecule containing only covalent bonds. 5) Rapamycin release from UM is sustainable at least for 2 months, consistent with our previous report [8]. 6) This painting method is easy and quick to apply without needing sophisticated devices - a feature critically important for a potential clinical utility and commercialization.

Conclusions

Currently, there is no approved therapy to prevent IH-associated postoperative failure of surgical reconstructions, which are commonly performed to treat atherosclerotic stenosis. In response to this critical medical need, we developed a painting modality for perivascular drug delivery to mitigate IH. Literally, with minimal manipulation, we may have turned the vessel adventitia into a self-serving drug reservoir for controlled release. This method is quick and easy in application, and effective in curbing injury-induced IH without causing tissue damage. However, IH in humans often develops in a background of other disease conditions and it may progress for a long term. In this regard, an encouraging clue can be found in our previous studies, namely, treating IH with rapamycin-loaded nanoparticles in rats could have an IH-mitigating effect extended beyond the end of drug release [8, 10]. Nevertheless, future research is warranted to further develop this painting modality, using UM formulations capable of more prolonged drug release and preclinical models with a human-like condition, such as hypercholesterolemic Zucker rats.

Supplementary Material

Refer to Web version on PubMed Central for supplementary material.

Acknowledgements

This work was supported by the National Institute of Health (NIH) grants R01HL143469, R01HL129785 (to K.C.K, S.G., and L.-W.G.), and R01HL133665 (to L.-W.G.), and Overseas Research Fellowships, The Uehara Memorial Foundation in Japan (to T.S.).

References

[1]. Benjamin Emelia J, Virani Salim S, Callaway Clifton W, Chamberlain Alanna M, Chang Alexander R, Cheng S, Chiuve Stephanie E, Cushman M, Delling Francesca N, Deo R, de Ferranti Sarah D, Ferguson Jane F, Fornage M, Gillespie C, Isasi Carmen R, Jiménez Monik C, Jordan Lori C, Judd Suzanne E, Lackland D, Lichtman Judith H, Lisabeth L, Liu S, Longenecker Chris T, Lutsey Pamela L, Mackey Jason S, Matchar David B, Matsushita K, Mussolino Michael

E, Nasir K, O'Flaherty M, Palaniappan Latha P, Pandey A, Pandey Dilip K, Reeves Mathew J, Ritchey Matthew D, Rodriguez Carlos J, Roth Gregory A, Rosamond Wayne D, Sampson Uchechukwu KA, Satou Gary M, Shah Svati H, Spartano Nicole L, Tirschwell David L, Tsao Connie W, Voeks Jenifer H, Willey Joshua Z, Wilkins John T, Wu Jason HY, Alger Heather M, Wong Sally S, Muntner P, Heart Disease and Stroke Statistics—2018 Update: A Report From the American Heart Association, Circulation 137(12) (2018) e67–e492. [PubMed: 29386200]

[2]. Herrington W, Lacey B, Sherliker P, Armitage J, Lewington S, Epidemiology of Atherosclerosis and the Potential to Reduce the Global Burden of Atherothrombotic Disease, Circ Res 118(4) (2016) 535–46. [PubMed: 26892956]

[3]. Fowkes FG, Aboyans V, Fowkes FJ, McDermott MM, Sampson UK, Criqui MH, Peripheral artery disease: epidemiology and global perspectives, Nat Rev Cardiol 14(3) (2017) 156–170. [PubMed: 27853158]

[4]. Kithcart AP, Beckman JA, ACC/AHA Versus ESC Guidelines for Diagnosis and Management of Peripheral Artery Disease: JACC Guideline Comparison, J Am Coll Cardiol 72(22) (2018) 2789–2801. [PubMed: 30497565]

[5]. de Vries MR, Quax PHA, Inflammation in Vein Graft Disease, Frontiers in Cardiovascular Medicine 5 (2018) 3. [PubMed: 29417051]

[6]. de Vries MR, Simons KH, Jukema JW, Braun J, Quax PHA, Vein graft failure: from pathophysiology to clinical outcomes, Nature reviews. Cardiology 13(8) (2016) 451–470. [PubMed: 27194091]

[7]. Harskamp RE, Lopes RD, Baisden CE, de Winter RJ, Alexander JH, Saphenous vein graft failure after coronary artery bypass surgery: pathophysiology, management, and future directions, Ann Surg 257(5) (2013) 824–33. [PubMed: 23574989]

[8]. Chen G, Shi X, Wang B, Xie R, Guo L-W, Gong S, Kent KC, Unimolecular Micelle-Based Hybrid System for Perivascular Drug Delivery Produces Long-Term Efficacy for Neointima Attenuation in Rats, Biomacromolecules 18(7) (2017) 2205–2213. [PubMed: 28613846]

[9]. Chen G, Wang Y, Xie R, Gong S, A review on core-shell structured unimolecular nanoparticles for biomedical applications, Adv Drug Deliv Rev 130 (2018) 58–72. [PubMed: 30009887]

[10]. Shi X, Chen G, Guo L-W, Si Y, Zhu M, Pilla S, Liu B, Gong S, Kent KC, Periadventitial Application of Rapamycin-Loaded Nanoparticles Produces Sustained Inhibition of Vascular Restenosis, PLOS ONE 9(2) (2014) e89227. [PubMed: 24586612]

[11]. Park TG, Degradation of poly(lactic-co-glycolic acid) microspheres: effect of copolymer composition, Biomaterials 16(15) (1995) 1123–30. [PubMed: 8562787]

[12]. Liu H, Slamovich EB, Webster TJ, Less harmful acidic degradation of poly(lacticco-glycolic acid) bone tissue engineering scaffolds through titania nanoparticle addition, Int J Nanomedicine 1(4) (2006) 541–545. [PubMed: 17722285]

[13]. Wang B, Chen G, Urabe G, Xie R, Wang Y, Shi X, Guo L-W, Gong S, Kent KC, A paradigm of endothelium-protective and stent-free anti-restenotic therapy using biomimetic nanoclusters, Biomaterials 178 (2018) 293–301. [PubMed: 29958152]

[14]. Akkapeddi P, Azizi S-A, Freedy AM, Cal PMSD, Gois PMP, Bernardes GJL, Construction of homogeneous antibody–drug conjugates using site-selective protein chemistry, Chemical Science 7(5) (2016) 2954–2963. [PubMed: 29997785]

[15]. Sam S, Touahir L, Salvador Andresa J, Allongue P, Chazalviel JN, Gouget-Laemmel AC, Henry de Villeneuve C, Moraillon A, Ozanam F, Gabouze N, Djebbar S, Semiquantitative Study of the EDC/NHS Activation of Acid Terminal Groups at Modified Porous Silicon Surfaces, Langmuir 26(2) (2010) 809–814. [PubMed: 19725548]

[16]. Meschaninova MI, Novopashina DS, Semikolenova OA, Silnikov VN, Venyaminova AG, Novel Convenient Approach to the Solid-Phase Synthesis of Oligonucleotide Conjugates, Molecules 24(23) (2019).

[17]. Zhao L, Chen G, Li J, Fu Y, Mavlyutov TA, Yao A, Nickells RW, Gong S, Guo L-W, An intraocular drug delivery system using targeted nanocarriers attenuates retinal ganglion cell degeneration, Journal of Controlled Release 247 (2017) 153–166. [PubMed: 28063892]

[18]. Wang B, Zhang M, Urabe G, Huang Y, Chen G, Wheeler D, Dornbos DJ 3rd, Huttinger A, Nimjee SM, Gong S, Guo L-W, Kent KC, PERK Inhibition Mitigates Restenosis and

Thrombosis: A Potential Low-Thrombogenic Antirestenotic Paradigm, JACC Basic Transl Sci 5(3) (2020) 245–263. [PubMed: 32215348]

[19]. Huang Y, Urabe G, Zhang M, Li J, Ozer HG, Wang B, Kent KC, Guo LW, Nullifying epigenetic writer DOT1L attenuates neointimal hyperplasia, Atherosclerosis 308 (2020) 22–31. [PubMed: 32799103]

[20]. Osbun JW, Ellenbogen RG, Chesnut RM, Chin LS, Connolly PJ, Cosgrove GR, Delashaw JB, Golfinos JG, Greenlee JDW, Haines SJ, Jallo J, Muizelaar JP, Nanda A, Shaffrey M, Shah MV, Tew JM, van Loveren HR, Weinand ME, White JA, Wilberger JE, A Multicenter, Single-Blind, Prospective Randomized Trial to Evaluate the Safety of a Polyethylene Glycol Hydrogel (Duraseal Dural Sealant System) as a Dural Sealant in Cranial Surgery, World Neurosurgery 78(5) (2012) 498–504. [PubMed: 22381303]

[21]. Krishnan S, Raj CJ, Robert R, Ramanand A, Das SJ, Growth and characterization of succinic acid single crystals, Crystal Research and Technology 42(11) (2007) 1087–1090.

[22]. Nair K L, Jagadeeshan S, Nair S A, Kumar GSV, Folic Acid Conjugated δ -Valerolactone-Poly(ethylene glycol) Based Triblock Copolymer as a Promising Carrier for Targeted Doxorubicin Delivery, PLOS ONE 8(8) (2013) e70697. [PubMed: 23990912]

[23]. Salva R, Le Meins JF, Sandre O, Brûlet A, Schmutz M, Guenoun P, Lecommandoux S, Polymersome shape transformation at the nanoscale, ACS Nano 7(10) (2013) 9298–311. [PubMed: 24047230]

[24]. Peng HT, Huang H, Shek PN, Charbonneau S, Blostein MD, PEGylation of Melittin: Structural Characterization and Hemostatic Effects, Journal of Bioactive and Compatible Polymers 25(1) (2010) 75–97.

[25]. Gao W, Zhang Y, Zhang Q, Zhang L, Nanoparticle-Hydrogel: A Hybrid Biomaterial System for Localized Drug Delivery, Ann Biomed Eng 44(6) (2016) 2049–2061. [PubMed: 26951462]

[26]. Suto T, Karonitsch T, The immunobiology of mTOR in autoimmunity, J Autoimmun 110 (2020) 102373. [PubMed: 31831256]

[27]. Almasri J, Adusumalli J, Asi N, Lakis S, Alsawas M, Prokop LJ, Bradbury A, Kolh P, Conte MS, Murad MH, A systematic review and meta-analysis of revascularization outcomes of infrainguinal chronic limb-threatening ischemia, J Vasc Surg 68(2) (2018) 624–633. [PubMed: 29804736]

[28]. Hess CN, Lopes RD, Gibson CM, Hager R, Wojdyla DM, Englum BR, Mack MJ, Califf RM, Kouchoukos NT, Peterson ED, Alexander JH, Saphenous vein graft failure after coronary artery bypass surgery: insights from PREVENT IV, Circulation 130(17) (2014) 1445–51. [PubMed: 25261549]

[29]. Al-Jaishi AA, Oliver MJ, Thomas SM, Lok CE, Zhang JC, Garg AX, Kosa SD, Quinn RR, Moist LM, Patency rates of the arteriovenous fistula for hemodialysis: a systematic review and meta-analysis, Am J Kidney Dis 63(3) (2014) 464–78. [PubMed: 24183112]

[30]. Schild AF, Perez E, Gillaspie E, Seaver C, Livingstone J, Thibonnier A, Arteriovenous fistulae vs. arteriovenous grafts: a retrospective review of 1,700 consecutive vascular access cases, J Vasc Access 9(4) (2008) 231–5. [PubMed: 19085891]

[31]. Goodney PP, Beck AW, Nagle J, Welch HG, Zwolak RM, National trends in lower extremity bypass surgery, endovascular interventions, and major amputations, J Vasc Surg 50(1) (2009) 54–60. [PubMed: 19481407]

[32]. Taggart DP, Ben Gal Y, Lees B, Patel N, Webb C, Rehman SM, Desouza A, Yadav R, De Robertis F, Dalby M, Banning A, Channon KM, Di Mario C, Orion E, A Randomized Trial of External Stenting for Saphenous Vein Grafts in Coronary Artery Bypass Grafting, Ann Thorac Surg 99(6) (2015) 2039–45. [PubMed: 25886810]

[33]. LoPachin RM, Gavin T, Molecular Mechanisms of Aldehyde Toxicity: A Chemical Perspective, Chemical Research in Toxicology 27(7) (2014) 1081–1091. [PubMed: 24911545]

[34]. Chivers CE, Koner AL, Lowe ED, Howarth M, How the biotin-streptavidin interaction was made even stronger: investigation via crystallography and a chimaeric tetramer, Biochem J 435(1) (2011) 55–63. [PubMed: 21241253]

[35]. Harris G, Ma W, Maurer LM, Potts JR, Mosher DF, Borrelia burgdorferi protein BBK32 binds to soluble fibronectin via the N-terminal 70-kDa region, causing fibronectin to undergo conformational extension, J Biol Chem 289(32) (2014) 22490–9. [PubMed: 24962582]

[36]. Jain M, Dhanesha N, Doddapattar P, Chorawala MR, Nayak MK, Cornelissen A, Guo L, Finn AV, Lentz SR, Chauhan AK, Smooth muscle cell–specific fibronectin-EDA mediates phenotypic switching and neointimal hyperplasia, The Journal of Clinical Investigation 130(1) (2020) 295–314. [PubMed: 31763999]

[37]. Kord Forooshani P, Lee BP, Recent approaches in designing bioadhesive materials inspired by mussel adhesive protein, Journal of Polymer Science Part A: Polymer Chemistry 55(1) (2017) 9–33.

[38]. Leichner C, Wulz P, Baus RA, Menzel C, Götzfried SK, Gust R, Bernkop-Schnürch A, N-Hydroxysulfosuccinimide Esters versus Thiomers: A Comparative Study Regarding Mucoadhesiveness, Molecular Pharmaceutics 16(3) (2019) 1211–1219. [PubMed: 30707584]

[39]. Nam K, Kimura T, Kishida A, Controlling Coupling Reaction of EDC and NHS for Preparation of Collagen Gels Using Ethanol/Water Co-Solvents, Macromolecular Bioscience 8(1) (2008) 32–37. [PubMed: 18023082]

[40]. Qazvini NT, Zinatloo S, Synthesis and characterization of gelatin nanoparticles using CDI/NHS as a non-toxic cross-linking system, J Mater Sci Mater Med 22(1) (2011) 63–9. [PubMed: 21052793]

[41]. Goel SA, Guo LW, Liu B, Kent KC, Mechanisms of post-intervention arterial remodelling, Cardiovasc Res 96(3) (2012) 363–71. [PubMed: 22918976]

[42]. Lynn AD, Kyriakides TR, Bryant SJ, Characterization of the in vitro macrophage response and in vivo host response to poly(ethylene glycol)-based hydrogels, J Biomed Mater Res A 93(3) (2010) 941–53. [PubMed: 19708075]

[43]. Rafuse M, Xu X, Stenmark K, Neu CP, Yin X, Tan W, Layer-specific arterial micromechanics and microstructure: Influences of age, anatomical location, and processing technique, J Biomech 88 (2019) 113–121. [PubMed: 31010593]

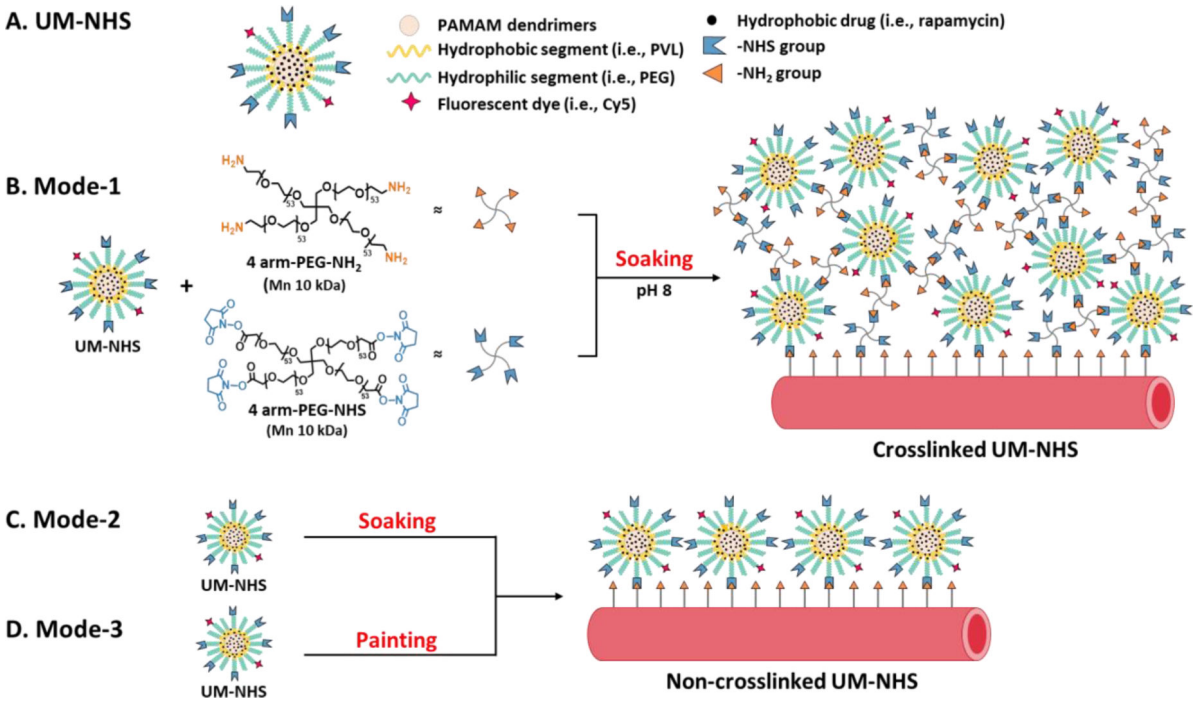

Figure 1.

Schematic illustration of the design and application of UM-NHS. (A) Schematic illustration of the chemical structure of UM-NHS. (B) Mode-1: UM-NHS crosslinked at pH 8.0 and its periadventitial application via soaking with the artery. (C) Mode-2: Periadventitial application of non-crosslinked UM-NHS via soaking with the artery. (D) Mode-3: Periadventitial application of non-crosslinked UM-NHS via pen-brush painting onto the artery.

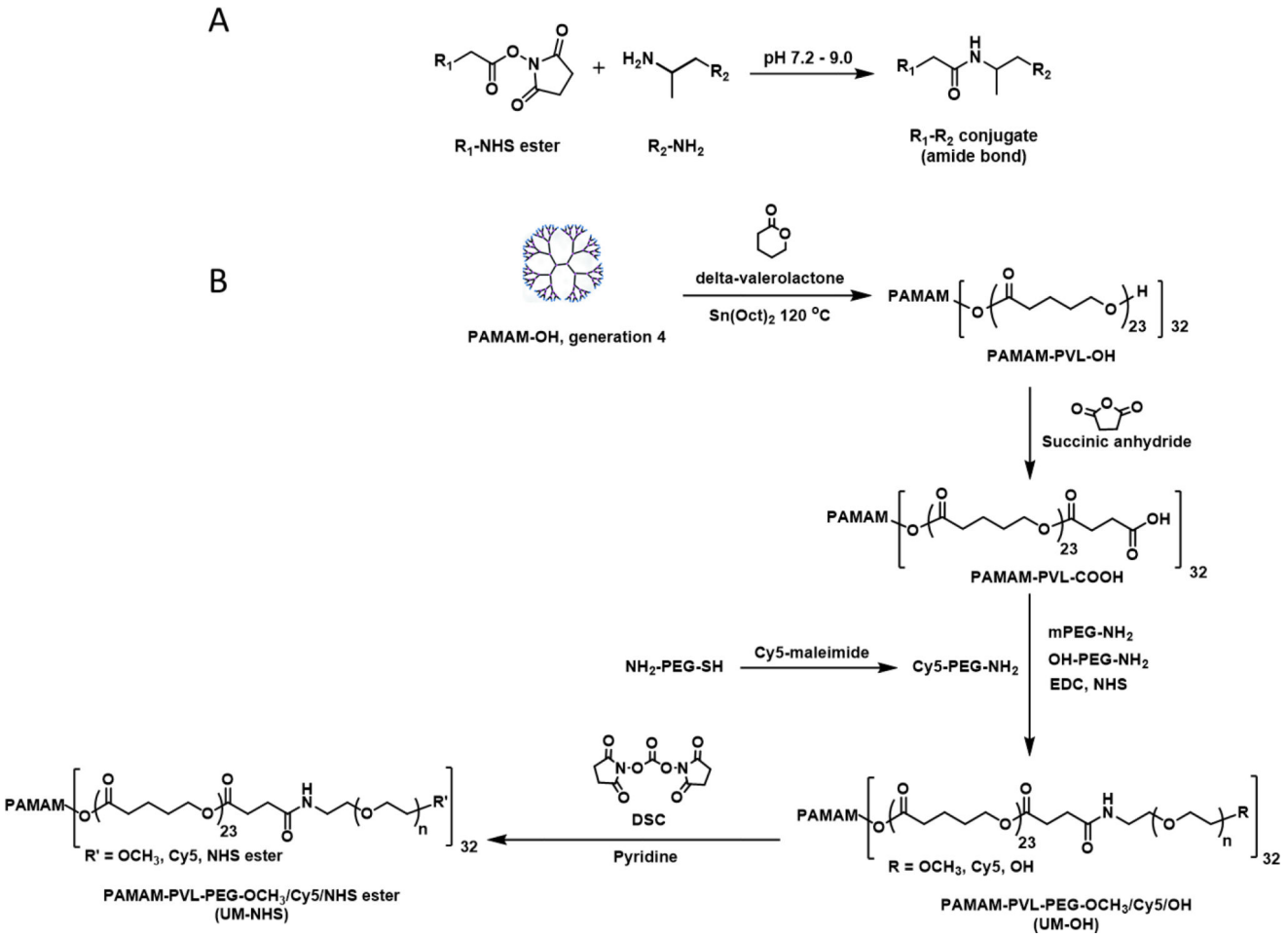

Figure 2.

(A) The reaction between NHS ester and amine under basic condition to generate a stable product with amide bond. (B) The synthetic procedure to yield PAMAM-PVL-PEG-NHS (UM-NHS) that can be used to react with amine on the vascular outer surface.

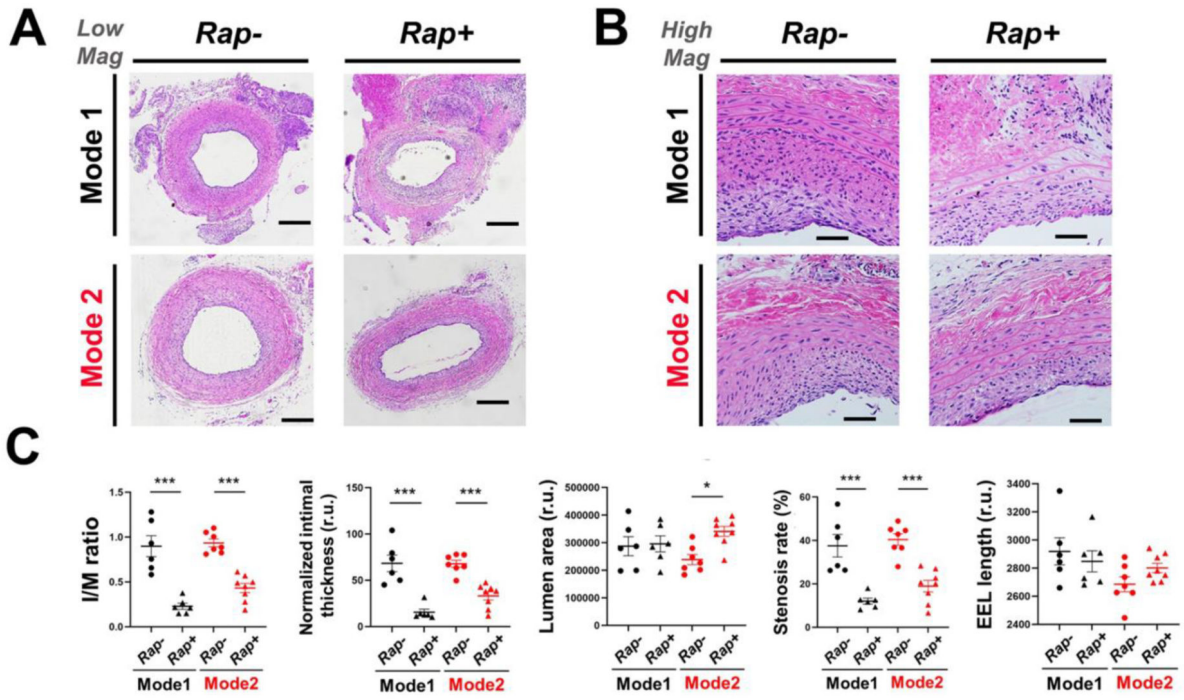

Figure 3. IH-mitigating effect of rapamycin periadventitially delivered through crosslinked (Mode-1) or non-crosslinked UM (Mode-2).

The open surgery of rat common carotid artery angioplasty followed by periadventitial application of UM (without or with rapamycin) was described in Methods. At post-surgery 14 days arteries were harvested for cross-section preparation and H&E staining. (A) Representative H&E-stained artery cross-sections. Scale bar: 200 μm. (B) High-mag images. Scale bar: 50 μm. (C) Morphometric quantification: mean ± SEM, n = 6–8 rats, as indicated by the data points in each plot. Statistics: ANOVA and Bonferroni test: *P <0.05. r.u., relative unit. The calculation of I/M ratio, normalized intimal thickness, and stenosis rate are described in Methods.

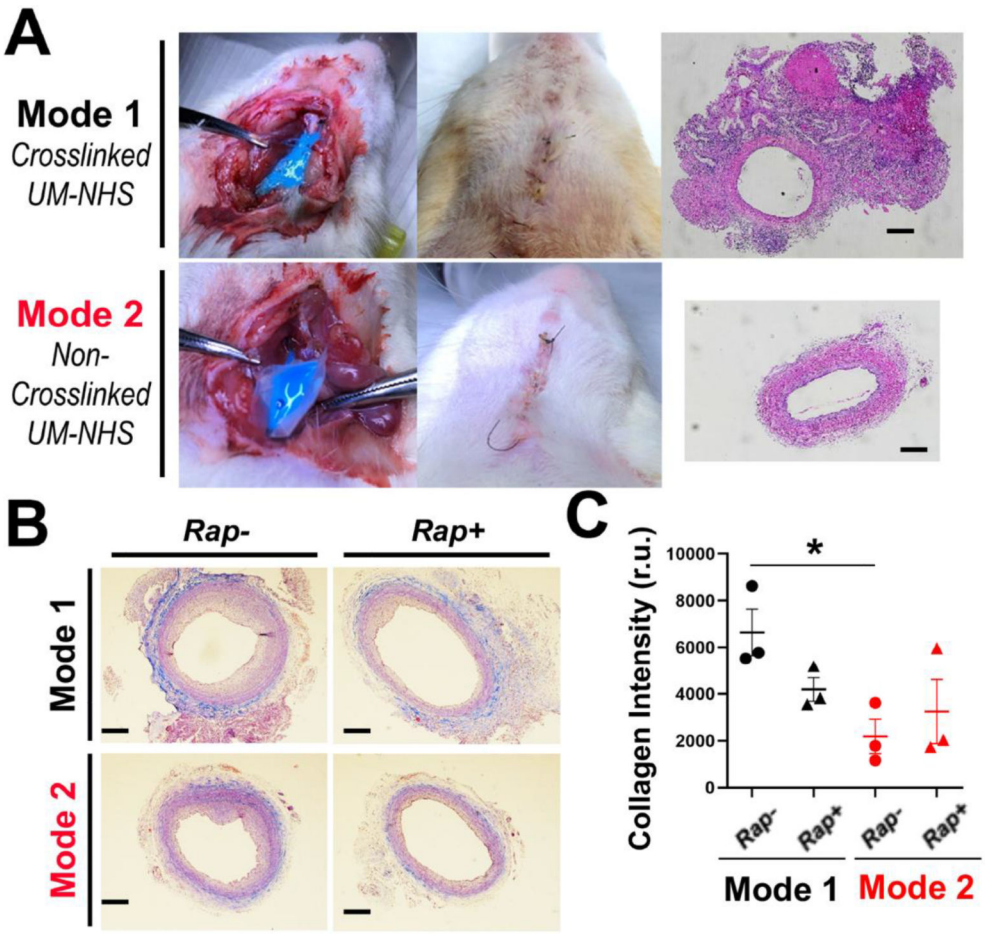

Figure 4. Pro-fibrotic effect of the Mode-1 (*vs* Mode-2) application on the artery.

(A) Photographic illustration of periadventitial application of UM. The photos show post-application (14 days) neck bulging in Mode-1 and lack of thereof in Mode-2. Note that the Cy5 fluorophore appeared blue at higher concentrations but not at lower concentrations (refer to Figure 6A). Shown on the right are representative H&E-stained cross-sections including undissectible surrounding tissues in Model-1. Scale bar: 200 μm. (B) Representative images of Masson's trichrome staining of artery cross-sections. Scale bar: 200 μm. (C) Quantification: mean ± SEM, n = 3 rats. Statistics: ANOVA and Bonferroni test: *P <0.05. r.u., relative unit.

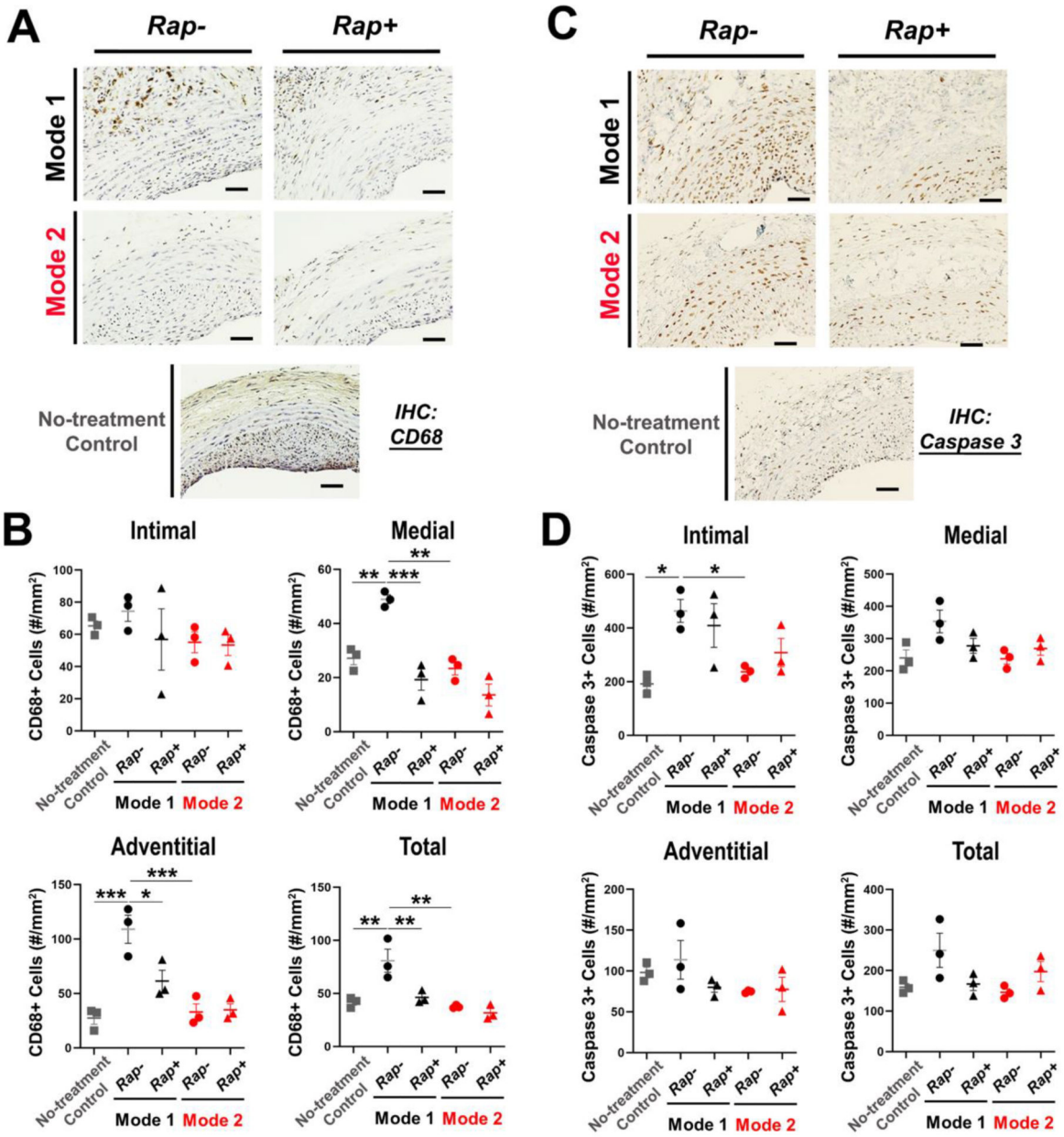

Figure 5. Pro-inflammatory/pro-apoptotic effect of the Mode-1 (*vs* Mode-2) application on the artery.

(A and B) Immunostaining of the inflammation marker CD68. Shown in A are representative staining images. Scale bar: 50 μm. Non-treatment control: no UM application. Quantification: mean ± SEM, n = 3 rats. Statistics: ANOVA and Bonferroni test: *P <0.05, **P<0.01, **P<0.001. (C and D) Immunostaining of the apoptosis marker active (cleaved) caspase-3. Shown in C are representative staining images. Scale bar: 50 μm. Non-treatment control: no UM application. Quantification: mean ± SEM, n = 3 rats. Statistics: ANOVA and Bonferroni test: *P <0.05.

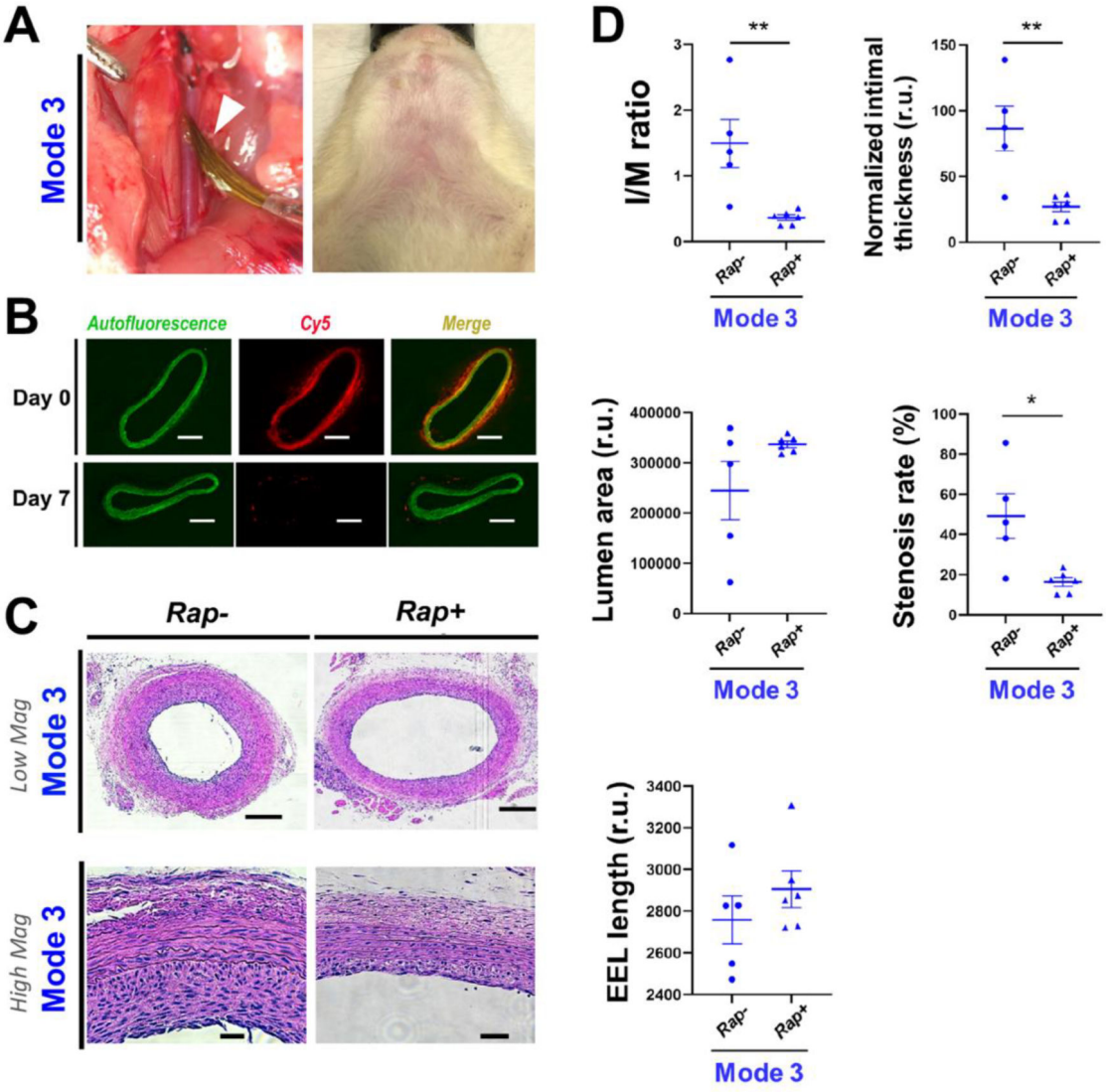

Figure 6. IH-mitigating effect of rapamycin periadventitially delivered using a painting approach (Mode-3).

Open surgery followed by periadventitial application of UM-NHS (without or with rapamycin) was described in Methods. At post-surgery 14 days arteries were harvested for cross-section preparation and H&E staining. (A) Photographic illustration of the UM-NHS painting approach (Mode-3). Left panel: Balloon-injured common carotid artery after painting UM-NHS with a pen brush (pointed by white arrow head). Note the painted UM-NHS appeared colorless. Right panel: Rat neck at post-surgery Day 14. Note the lack of neck bulging. (B) Representative images of Cy5 fluorescence from artery cross-sections. Cy5 was conjugated on UM. Images were taken on the sections of arteries collected right after UM application (day 0) or 7 days post application (day 7). Autofluorescence from elastic laminae profiles the medial layer. Scale bar: 200 μm. (C) Representative H&E-stained artery cross-sections. Scale bar: 200 μm (low mag), 50 μm (high mag). (D) Morphometric quantification: mean ± SEM, n = 6 rats. Statistics: Student t-test: *P <0.05, **P<0.01. r.u.,

relative unit. The calculation of I/M ratio, standardized intimal thickness, and stenosis rate is described in Methods.

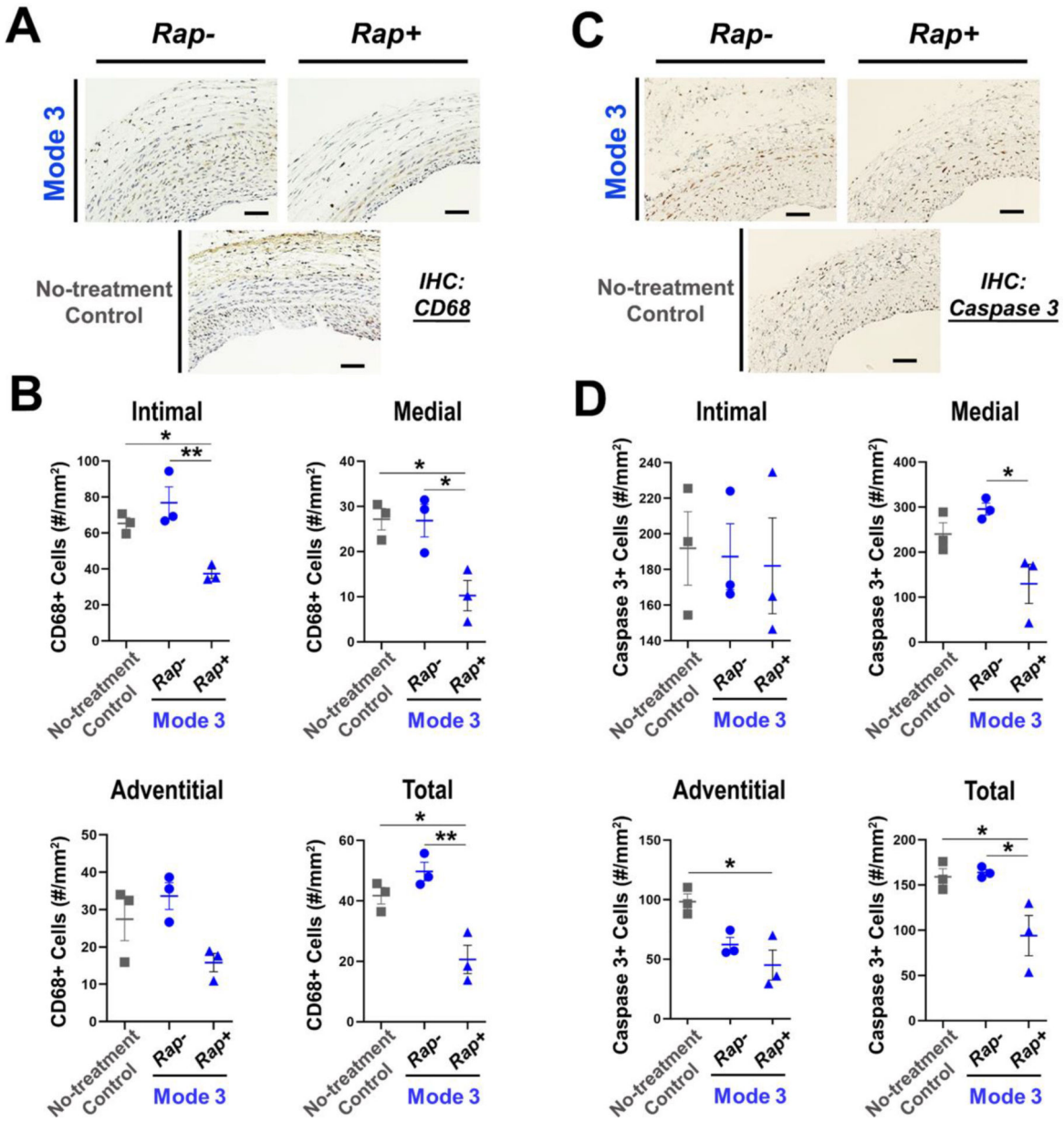

Figure 7. Determination of the tissue toxicity of the Mode-3 formulations.

(A and B) Immunostaining of the inflammation marker CD68. Shown in A are representative staining images. Scale bar: 50 μm. Non-treatment control: no UM application. Quantification: mean ± SEM, n = 3 rats. Statistics: ANOVA and Bonferroni test: *P <0.05, **P<0.01. (C and D) Immunostaining of the apoptosis marker active (cleaved) caspase-3. Shown in C are representative staining images. Scale bar: 50 μm. Non-treatment control: no UM application. Quantification: mean ± SEM, n = 3 rats. Statistics: ANOVA and Bonferroni test: *P <0.05.